106

SATELLITE & MESOMETEOROLOGY RESEARCH PROJECT

Department of the Geophysical Sciences
The University of Chicago

USE OF ATS PICTURES IN HURRICANE MODIFICATION

by

T. Theodore Fujita

SMRP Research Paper

August 1972

MESOMETEOROLOGY PROJECT --- RESEARCH PAPERS

1.* Report on the Chicago Tornado of March 4, 1961 - Rodger A. Brown and Tetsuya Fujita

2.* Index to the NSSP Surface Network - Tetsuya Fujita

3.* Outline of a Technique for Precise Rectification of Satellite Cloud Photographs - Tetsuya Fujita

4.* Horizontal Structure of Mountain Winds - Henry A. Brown

5.* An Investigation of Developmental Processes of the Wake Depression Through Excess Pressure Analysis of Nocturnal Showers - Joseph L. Goldman

6.* Precipitation in the 1960 Flagstaff Mesometeorological Network - Kenneth A. Styber

7.** On a Method of Single- and Dual-Image Photogrammetry of Panoramic Aerial Photographs - Tetsuya Fujita

8. A Review of Researches on Analytical Mesometeorology - Tetsuya Fujita

9.* Meteorological Interpretations of Convective Nephsystems Appearing in TIROS Cloud Photographs - Tetsuya Fujita, Toshimitsu Ushijima, William A. Hass, and George T. Dellert, Jr.

10.* Study of the Development of Prefrontal Squall-Systems Using NSSP Network Data - Joseph L. Goldman

11. Analysis of Selected Aircraft Data from NSSP Operation, 1962 - Tetsuya Fujita

12. Study of a Long Condensation Trail Photographed by TIROS I - Toshimitsu Ushijima

13. A Technique for Precise Analysis of Satellite Data; Volume I - Photogrammetry (Published as MSL Report No. 14) - Tetsuya Fujita

14. Investigation of a Summer Jet Stream Using TIROS and Aerological Data - Kozo Ninomiya

15. Outline of a Theory and Examples for Precise Analysis of Satellite Radiation Data - Tetsuya Fujita

16. Preliminary Result of Analysis of the Cumulonimbus Cloud of April 21, 1961 - Tetsuya Fujita and James Arnold

17. A Technique for Precise Analysis of Satellite Photographs - Tetsuya Fujita

18.* Evaluation of Limb Darkening from TIROS III Radiation Data - S.H.H. Larsen, Tetsuya Fujita, and W.L. Fletcher

19. Synoptic Interpretation of TIROS III Measurements of Infrared Radiation - Finn Pedersen and Tetsuya Fujita

20.* TIROS III Measurements of Terrestrial Radiation and Reflected and Scattered Solar Radiation - S.H.H. Larsen, Tetsuya Fujita, and W.L. Fletcher

21. On the Low-level Structure of a Squall Line - Henry A. Brown

22.* Thunderstorms and the Low-level Jet - William D. Bonner

23.* The Mesoanalysis of an Organized Convective System - Henry A. Brown

24. Preliminary Radar and Photogrammetric Study of the Illinois Tornadoes of April 17 and 22, 1963 - Joseph L. Goldman and Tetsuya Fujita

25. Use of TIROS Pictures for Studies of the Internal Structure of Tropical Storms - Tetsuya Fujita with Rectified Pictures from TIROS I Orbit 125, R/O 128 - Toshimitsu Ushijima

26. An Experiment in the Determination of Geostrophic and Isallobaric Winds from NSSP Pressure Data - William Bonner

27. Proposed Mechanism of Hook Echo Formation - Tetsuya Fujita with a Preliminary Mesosynoptic Analysis of Tornado Cyclone Case of May 26, 1963 - Tetsuya Fujita and Robbi Stuhmer

28. The Decaying Stage of Hurricane Anna of July 1961 as Portrayed by TIROS Cloud Photographs and Infrared Radiation from the Top of the Storm - Tetsuya Fujita and James Arnold

29. A Technique for Precise Analysis of Satellite Data, Volume II - Radiation Analysis, Section 6. Fixed-Position Scanning - Tetsuya Fujita

30. Evaluation of Errors in the Graphical Rectification of Satellite Photographs - Tetsuya Fujita

31. Tables of Scan Nadir and Horizontal Angles - William D. Bonner

32. A Simplified Grid Technique for Determining Scan Lines Generated by the TIROS Scanning Radiometer - James E. Arnold

33. A Study of Cumulus Clouds over the Flagstaff Research Network with the Use of U-2 Photographs - Dorothy L. Bradbury and Tetsuya Fujita

34. The Scanning Printer and Its Application to Detailed Analysis of Satellite Radiation Data - Tetsuya Fujita

35. Synoptic Study of Cold Air Outbreak over the Mediterranean using Satellite Photographs and Radiation Data - Aasmund Rabbe and Tetsuya Fujita

36. Accurate Calibration of Doppler Winds for their use in the Computation of Mesoscale Wind Fields - Tetsuya Fujita

37. Proposed Operation of Intrumented Aircraft for Research on Moisture Fronts and Wake Depressions - Tetsuya Fujita and Dorothy L. Bradbury

38. Statistical and Kinematical Properties of the Low-level Jet Stream - William D. Bonner

39. The Illinois Tornadoes of 17 and 22 April 1963 - Joseph L. Goldman

40. Resolution of the Nimbus High Resolution Infrared Radiometer - Tetsuya Fujita and William R. Bandeen

41. On the Determination of the Exchange Coefficients in Convective Clouds - Rodger A. Brown

* Out of Print
** To be published

(Continued on back cover)

USE OF ATS PICTURES IN HURRICANE MODIFICATION

by

T. Theodore Fujita
Department of the Geophysical Sciences
The University of Chicago

SMRP Research Paper No. 106
August 1972

The research reported in this paper was sponsored by the National Hurricane Research Laboratory under grant N 22-21-72 (G).

USE OF ATS PICTURES IN HURRICANE MODIFICATION[1]

by

T. Theodore Fujita
The University of Chicago

Abstract

ATS pictures taken at frequent intervals during a 4-day period, September 25-28, were analyzed in an attempt to determine possible changes of Hurricane Ginger seeded on September 26 and 28. Both NESS negatives and NASA's 4X enlargements from digital tapes were investigated. All pictures taken on each day were time-integrated to determine the day-to-day variations. One-day sequence of ATS pictures were also divided into three periods to produce 3 time-integrated images each day. Series of 5-picture time integrations were also made, from which a time-integrated movie of Ginger was produced. Meanwhile, the characteristics of the eye were determined based on ATS pictures to define a number of eye parameters which are eye type, wall-cloud diameter, equivalent eye diameter, eye index, and estimated central pressure. Despite these efforts conclusive evidence of modification effects has not been found in ATS pictures reduced in various forms. It is, thus, assumed that Ginger of 1971 was too weak and too low in convective cloud-top heights to respond significantly to the seeding experiment.

1. INTRODUCTION

Since the multiple seeding experiments of Hurricane Debbie conducted on August 18 and 20, 1969, various methods of evaluating expected effects of seeding were explored by Project Stormfury. As predicted in Simpson's 1961 hypothesis, the maximum windspeeds in Debbie decreased significantly soon after the multiple seedings. Furthermore, most of the damage from hurricanes is caused by either the winds or the wind driven storm tide. The wind fields, therefore, have become the primary method of evaluating the effects of hurricane seeding.

---

[1] The research reported in this paper was sponsored by National Hurricane Research Laboratory under grant N 22-21-72 (G).

As explained in Appendix B of the 1970 Annual Report of Project Stormfury (1971), Gentry hypothesized an onset of a bigger chain reaction involving condensation of extra water vapor. The stimulation of cloud growth through expected chain reaction will allow upward transport of inflow air into the outflow layer, resulting thus in a further expansion of the eyewall. Such a variation in the pattern of clouds within and surrounding the eyewall can be determined by careful examination of radar echoes and their motion. Despite the argument that echo velocity does not always represent the environmental air motion, Black (1971) demonstrated the potential values of echo motions for estimating overall modification effects. Aerial photographs taken from U-2 or RB 57 altitudes will also be of value if they can be analyzed properly to obtain net variations of cloud patterns due to seeding.

ATS pictures available for every 12 to 27 minutes during the period of Stormfury Experiments will add further information on the overall patterns of the eyewall circulation. It is the purpose of this paper to explore the possibilities of evaluating both expected and unexpected changes in the cloud patterns during the Stormfury Experiment.

2. LIFE HISTORY OF HURRICANE GINGER

During the 1971 hurricane season, hurricane Ginger was seeded by Project Stormfury. Characteristics of this hurricane along with other Atlantic hurricanes were presented by Simpson and Hope (1972). They stated that Ginger was tracked for 31 days, during 20 of which it was a hurricane. Ginger was the longest-life hurricane in the Atlantic (see Fig. 1).

During the long lifetime of the storm, the central pressure of Ginger showed two major periods of minimum central pressure on September 13 and 27, some two weeks apart. Between these periods the central pressure gradually rose and fell with a rather flat maximum lasting for about one week. Two seeding periods, indicated with letter "S", are seen on September 26 and 28. These days are found within the second minimum period of the central pressure in which the central pressure turned out to be rather unsteady, characterized by pressure oscillations with 2-day period. On October 1, Ginger landed on the Carolina coast while filling and weakening very rapidly.

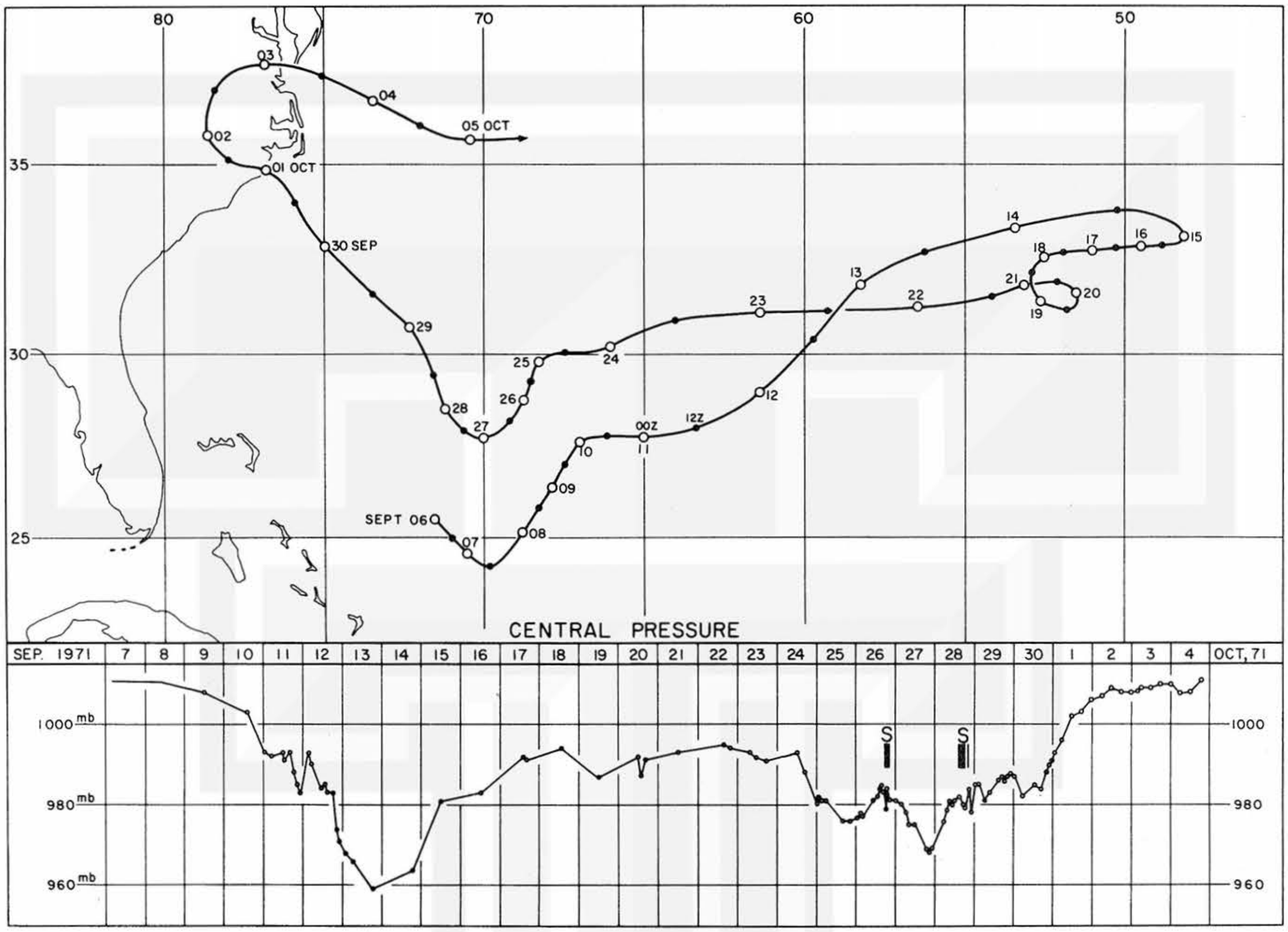

Figure 1. Track of hurricane Ginger, Sept. 6 through Oct. 5 from Simpson and Hope (1972) and the variation of the central pressure. The periods of seeding on Sept. 26 and 27 are identified with letter "S".

3. ATS III VIEWS OF GINGER

For a five-day period between September 25-29, 1971 digital tapes including the full resolution of ATS III pictures were made by NASA at Wallops Island readout station. Tapes were recorded concurrently with NOAA pictures made operationally at NESS in Suitland.

Presented in Fig. 2 are the enlargements of two images enlarged from NOAA's 9-inch negative and NASA's 4X enlargement on 4" x 5" negative from EIS machine at Goddard Space Flight Center. Since 4X enlargement is capable of reproducing almost full-resolution of ATS pictures, the lower picture shows more detailed view

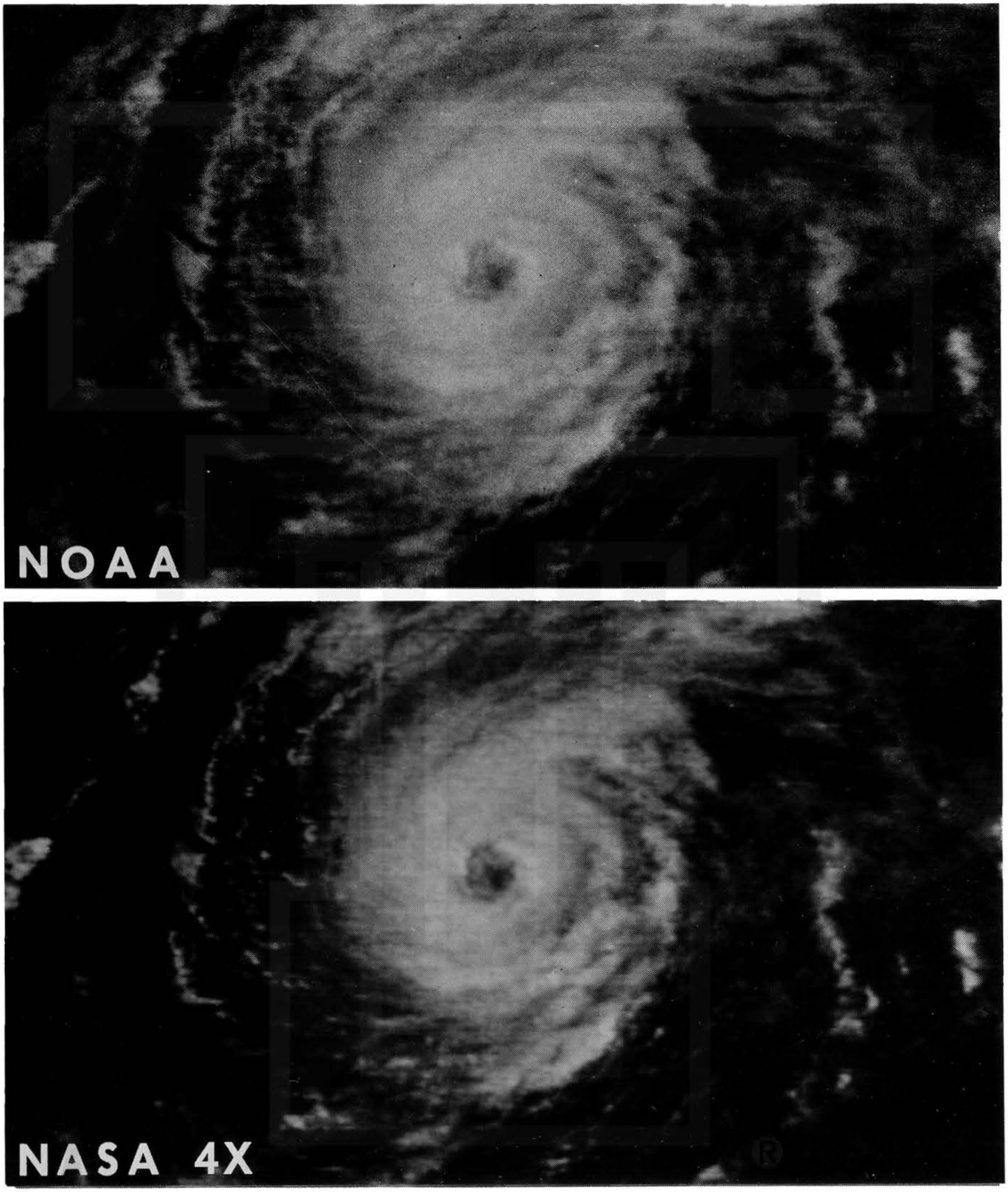

Figure 2. Comparison of ATS III pictures, frame 26, 1958 GMT, Sept. 27, 1971. The top picture was enlarged from NOAA negative and the bottom, from 4X negative produced by EIS machine at GSFC, NASA.

of Ginger's eye surrounded by convective towers along the eyewall. Ginger was a weak hurricane with the eyewall consisting more or less of terminating ends of several cloud- or rainbands. In this picture there are three such cloudbands, the first one terminating at the west wall with 3 distinct towers, the second one at the north wall with several high towers north through east sides of the wall, and the third, entering the eyewall from the south to the east sector. The eye itself was partially filled with decks of low and middle clouds, on top of which two towers on the west wall cast distinct shadows.

An attempt was made to locate the seeding areas on ATS pictures on September 26. Identification of the areas were made jointly with Mr. Peter Black of NHRL for the purpose of finding the relative position of the seeding aircraft and the major cloudband feeding into the eye wall. A detailed description of the seeding areas is given in Appendix B of the 1971 Stormfury Report by Hawkins, Bergman, and Gentry (1972).

Area A-1 seeded at 1701-1717 is shown in Fig. 3 on ATS pictures taken at 1702 and 1713 GMT. On the 1647 GMT picture, the scale of 100 nautical miles applicable to all pictures is indicated. It will be found that the A-1 seeding took place within the largest cloudband to the south of the eye. The initial point of the seeding at 1701 was 89.5-nm range and 175-deg range from the storm center. The relative wind measured by NHRL was about 60 kt, suggesting that the released silver iodide and its effect would propagate downwind at about this rate of speed.

The east-end point of the seeding at 1701, as identified with letter "a", was advected at 60 kt in the direction of the cloudband to show its successive positions in Fig. 3. No identifiable cloud feature was found to move with this point "a". There was, however, an elliptic area of fuzzy cloud which started showing up at 1713 to the east of the eye. The fuzzy cloud identified with letter "A" in the pictures started expanding radially outward as "a" approached. The translational speed of "A" was only about 30 kt while "a" advected at 60 kt. As a result, "a" caught up with the slow-moving "A" at 1822.

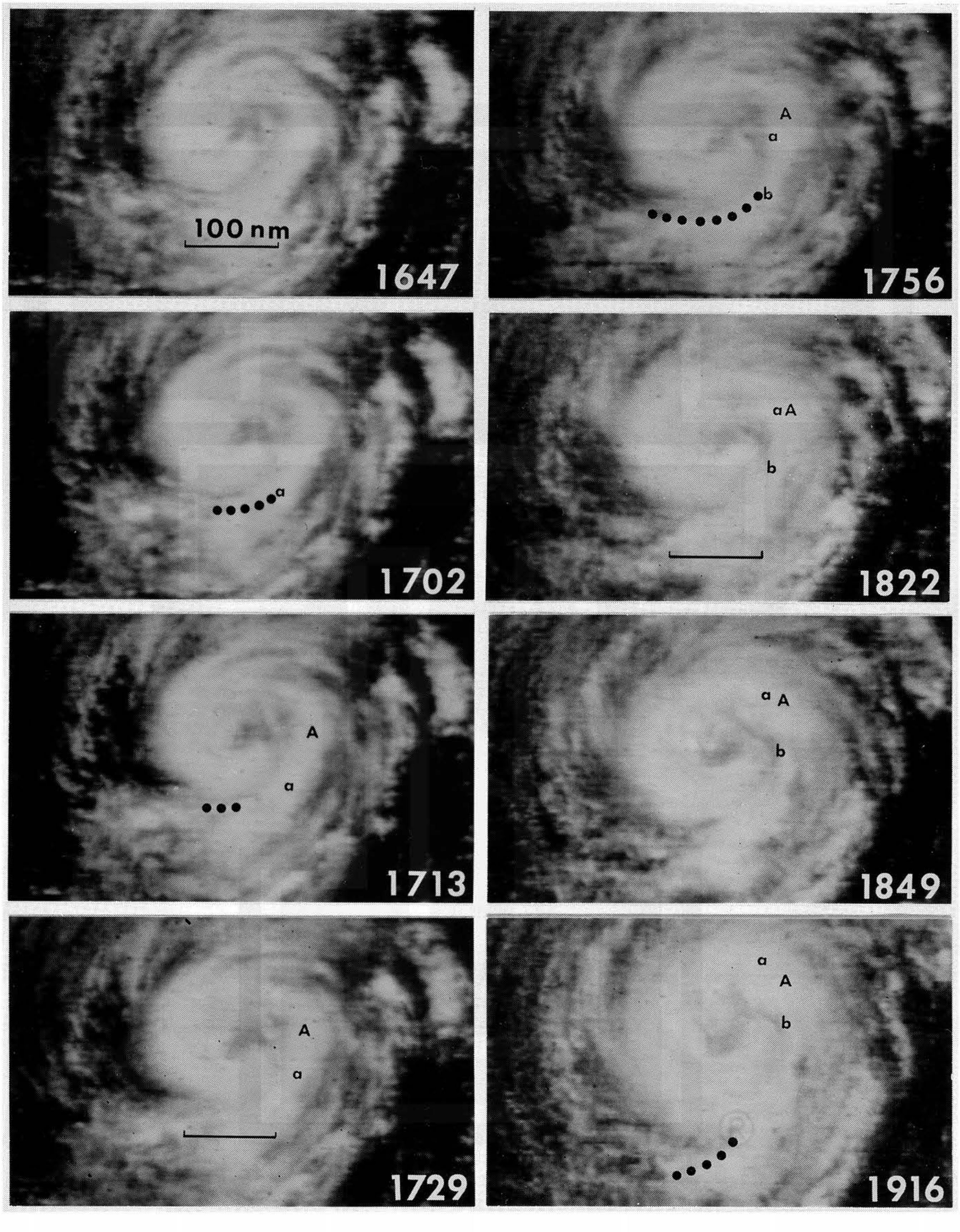

Figure 3. ATS III pictures showing the seeding locations on Sept. 26, 1971. "a" and "b" are the end point of seedings advected at 60 kt. Note that cloud "A" expanded as "a" went through it.

When the growth rate of "A" is examined closely together with the motion of "a", it will be found that the outburst of "A" took place when "a" got into the area of "A". In fact the equivalent diameter of "A" at 1756, which was about 60 nm, changed into 80 nm at 1916 some 80-minutes later. This rate of expansion will be about 15 kt outward because the inward growth of cloud "A" was negligibly small.

Since we do not know the vertical extent of cloud "A", it is not feasible to determine the cause of its growth attributed to the seeding. All we may say at the present time is that (1) the fuzzy cloud expanded radially approximately at the time when seeded point advected into the cloud area and that (2) there were no other clouds within the hurricane areas in Fig. 3 which grew as rapidly as this fuzzy cloud did.

The second part of the seeding A or A-2 seeding was made between 1734 and 1754. The end point of this seeding, identified with letter "b", was also advected in a similar manner to that of "a". The ATS picture sequence in Fig. 3 reveals that the point "b" was at the south edge of the fuzzy cloud at 1916.

It is unfortunate that the sequences of 4X enlargements by NASA were interrupted by "bad pictures" resulting from the sensitive pick up of noise which did not affect NOAA pictures appreciably. The noise situation became worse on the 28th when the second-day seeding was performed. In view of this undesirable result, the tape-recording speed at Wallops was arranged to slow down; meanwhile the EIS machine at GSFC was readjusted to insure better pictures for future hurricane modification.

4. VARIATION OF EYE

When a seeded hurricane undergoes changes based on the modification hypotheses, a new eyewall will develop at a greater radius. The inflow air entering this new eyewall is diverted upward before entering into the region of the old eyewall.

It is expected, therefore, that the diameter of the eyewall expands along with the reduction of the maximum tangential windspeed due mainly to the fact that the inflow air rises upward before it gains angular velocity by reducing the radius vector turning around the center.

In order to detect these hypothetical variations of both eyewall diameters and characteristics, ATS pictures taken during a 4-day period, September 25-28, were examined. As shown in Fig. 4, axes of cloudband and eye areas on each picture were traced. Cloudband axis is defined as the line along the brightness center of a banded cloud mostly spiraling around the eye. The eye area is very hard to define, unless an eye appears to be a circular clear area within a closed eyewall cloud. In the case of Ginger, the eyewall was incomplete, consisting of terminating ends of a number of rain- or cloudbands. The area of the eye was, therefore, defined as that of relatively dark portion within an incomplete eyewall. The boundary of approximately 50% brightness on enlarged ATS picture was traced and painted in order to identify the eye area.

Figures 4 through 7, covering the 4 day period, were thus completed. In producing these figures, no continuity between successive pictures was taken into consideration because the changes in the eye area were sometimes so large, necessitating analysis of individual pictures independently from others. After all, a total number of 114 pictures were examined to produce these figures.

The characteristics of the eye in each picture were then classified into six categories: a, b, c, d, e, and f. Their specifications are given in Table I.

Table I. Six categories of the eye characteristics

Eye Category	Characteristics
a	circular eye and wall cloud with clear eye inside
b	circular eyewall with relatively white eye areas
c	distorted eyewall with relatively clear eye
d	distorted eyewall with rather white eye area
e	irregular eyewall with clear spots inside
f	eye is not visible

Meanwhile the diameter of wall cloud, called the "Wall Cloud Diameter", was defined as being the equivalent diameter of either complete or incomplete axis of the wall cloud seen in ATS picture at a given time. The "Equivalent Eye Diameter" is the diameter of the circle whose area is equal to that of the total eye area within the wall cloud at a given time. These parameters are, then, designated by

C ..... Wall Cloud Diameter
E ..... Equivalent Eye Diameter

which are to be measured as functions of time. Experimental estimates of C and E revealed, however, that their variations with time is often so large that each of them should be smoothed in order to suppress their measurement error.

A running mean procedure was adopted to define the 2-hr running means,

$$\overline{C} = \frac{1}{2}\int_{t-1hr}^{t+1hr} C\,dt \quad \ldots \text{ Mean wall-cloud diameter}$$

$$\overline{E} = \frac{1}{2}\int_{t-1hr}^{t+1hr} E\,dt \quad \ldots \text{ Mean eye diameter}$$

The ratio of above mean diameters

$$\overline{Y} = \overline{E}/\overline{C}$$

which may be called the "eye index" was introduced to determine if these parameters can be used for evaluations of modification effects or not. The eye index, thus, defined is a measure of the clearing inside an eyewall. If the eye inside the eyewall is either completely clear or scattered with insignificant amount of cloud, $\overline{Y}$ may increase up to 1.0. Very strong descending motion inside the eye of a well-developed hurricane may result in such a large value of $\overline{Y}$. If, on the other hand, a hurricane is weak with insignificant eye, $\overline{Y}$ can be as small as zero, for which the eye is completely closed.

As presented in Tables II through V, various characteristics of Ginger's eye appearing in each ATS III picture were measured and tabulated.

Based on these tables, the eye indices, $\overline{Y}$, were first sorted at 0.1 intervals to determine its variation with $\overline{C}$, the mean wall-cloud diameter. It was quickly found that the central pressure reported by aircraft increases with $\overline{C}$ for a given 0.1 increment range of $\overline{Y}$. Figure 8 was, thus, produced by sorting both $\overline{C}$ and $\overline{Y}$ for every 10 nm and 0.1 respectively. The average value of $\overline{C}$ and $\overline{Y}$ within each box in the figure is indicated with a "+" symbol. The average central pressure corresponding to the data points within each box was also computed and entered in the figure. It is seen that the central pressure of Ginger increases with $\overline{C}$ but decreases with $\overline{Y}$, suggesting that a group of isolines of central pressures can be drawn in the figure. The central pressure thus determined from $\overline{Y}$ and $\overline{C}$ is called the "estimated central pressure", $\overline{P}_c$, which is the central pressure estimated from the time-averaged wall-cloud diameters and equivalent eye diameters measured on ATS pictures. Figure 8 will now permit us to estimate the central pressure based on the characteristic eyes in ATS pictures.

To summarize the variation of the eye characteristics of Ginger, Fig. 9 was constructed. The painted circles in the upper diagram are the central pressures from aircraft reports. Their trend of variation is expressed by a smoothed curve with three major maxima on September 25, 26 and 28. This curve was used to read off P_c , the central pressures given in Tables II through V as a function of ATS III picture time. For comparison purposes, the estimated central pressures, $\overline{P}_c$, are shown with open circles.

The middle diagram of Fig. 9 reveals the variation of the eye types classified into 6 categories. Two curves in the lower diagram give the tendency of the variation of wall-cloud and equivalent eye diameters.

Examination of Fig. 8 reveals that the central pressure of Ginger during the sun-lit hours of 25th was lower than that of 26th, the day of the first seeding. Both aircraft reports and ATS III estimates show the deepening on the 27th, followed by a steady incrase until the start time of the 28th seeding. During the 28th seeding the central pressure dropped several millibars but it started rising again toward the end of the day .

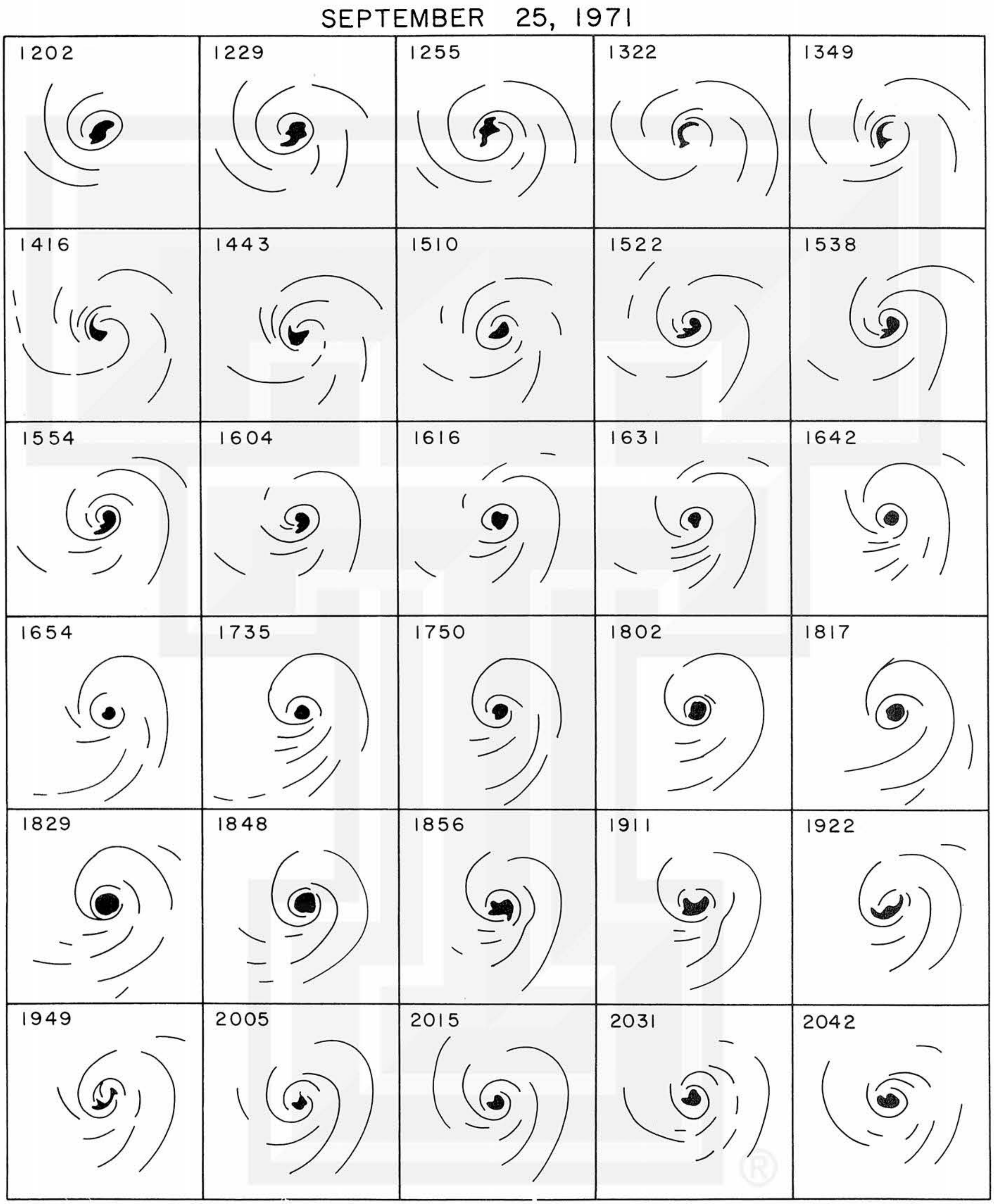

Figure 4. Schematic patterns of Ginger's eye and cloud band on Sept. 25, 1971. Each area covers 400-nm square.

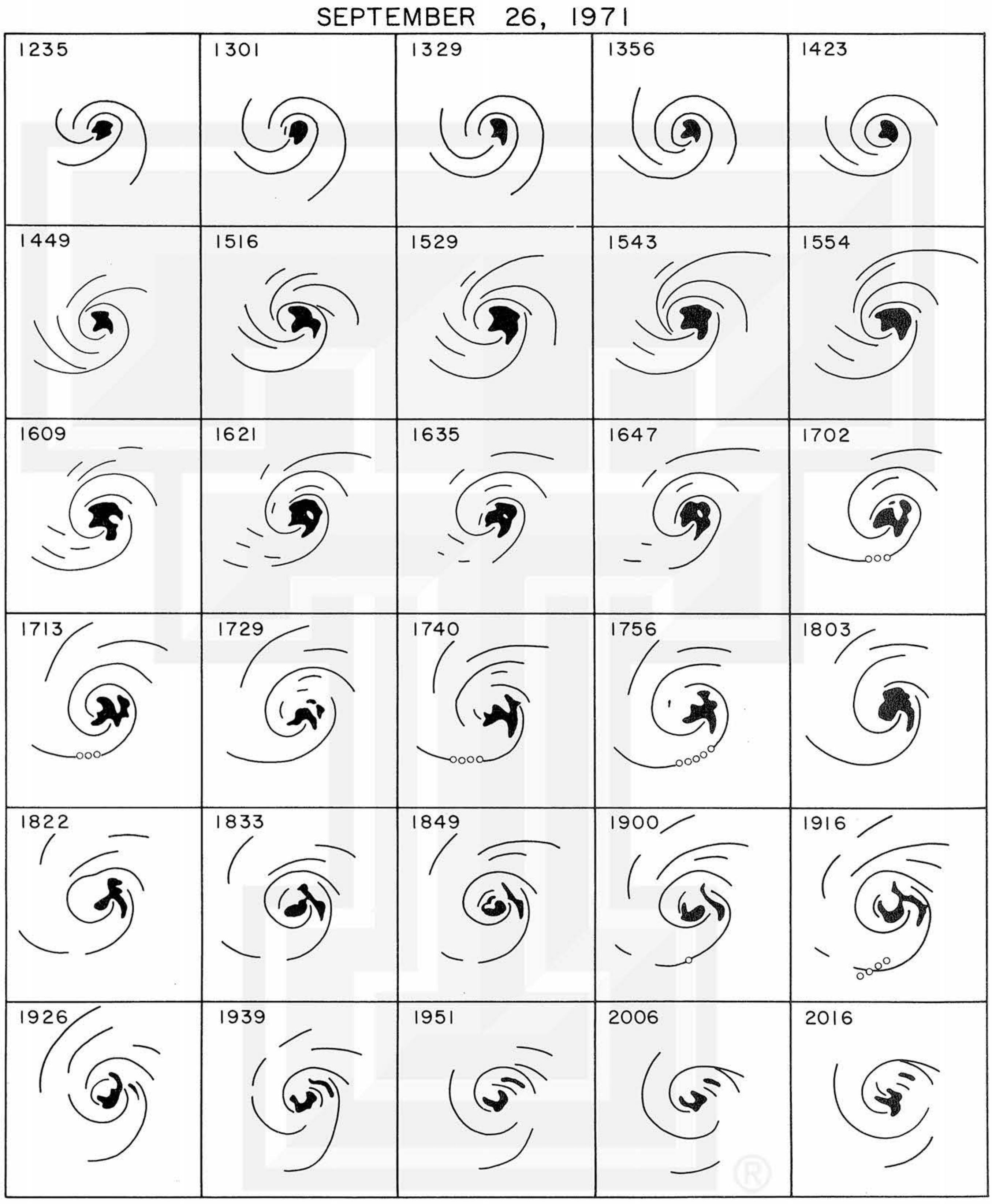

Figure 5, Schematic patterns of Ginger's eye and cloud band on Sept. 26, 1971. Each area covers 400-nm square. Locations of seeding are indicated by small open circles.

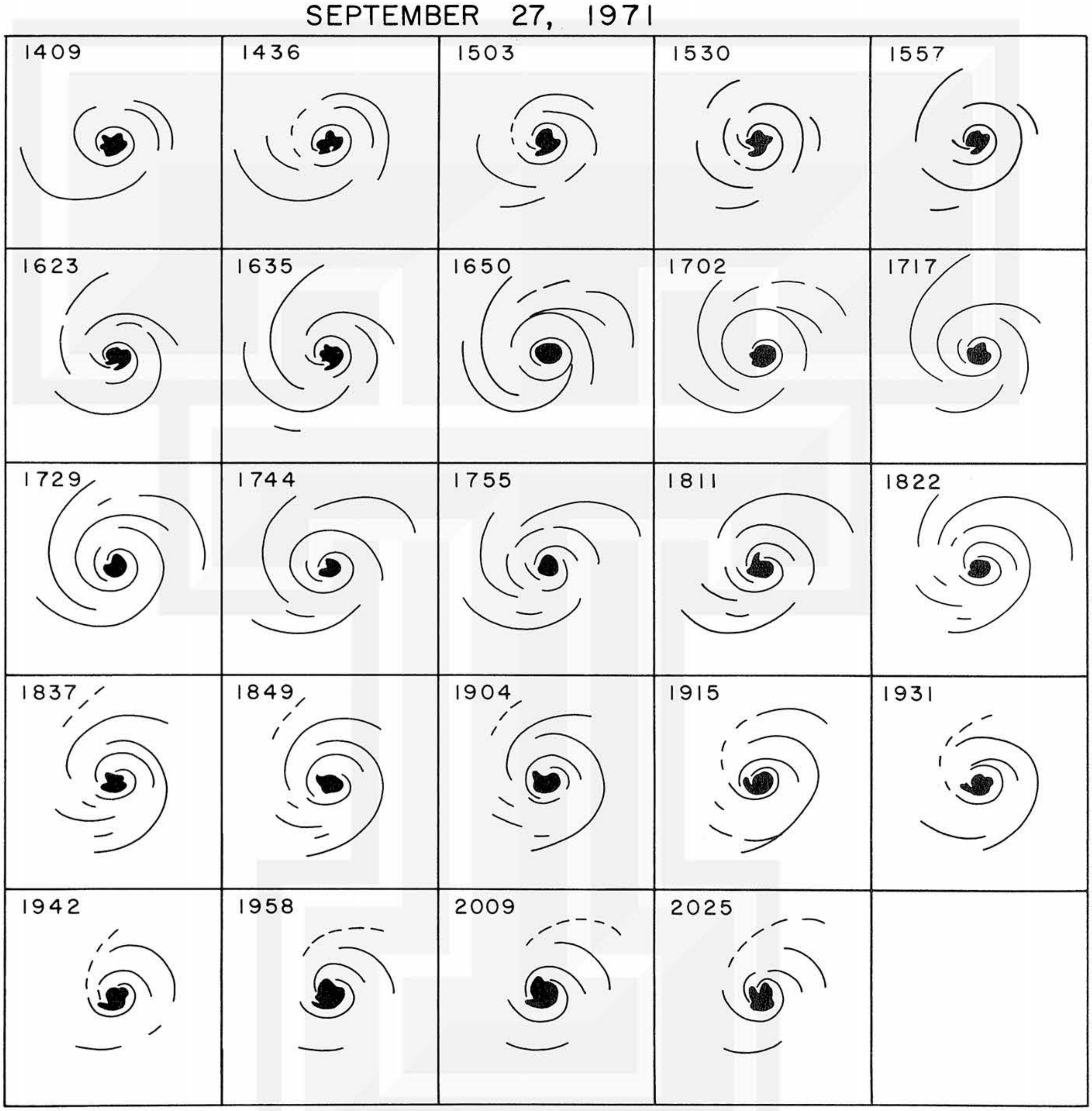

Figure 6. Schematic patterns of Ginger's eye and cloud band on Sept. 27, 1971. Each area covers 400-nm square.

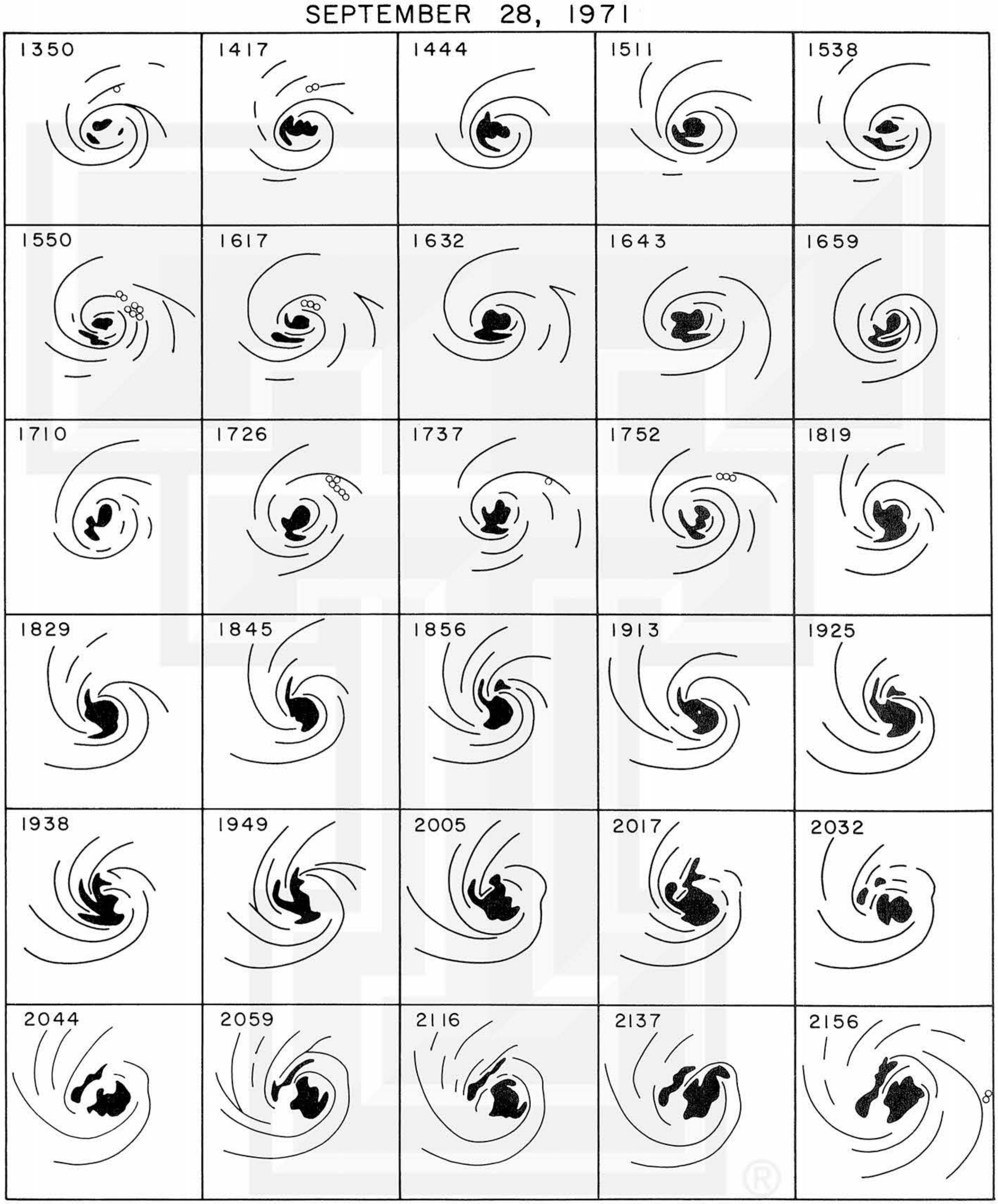

Figure 7. Schematic patterns of Ginger's eye and cloud band on Sept. 28, 1971. Each area covers 400-nm square. Locations of seeding are indicated by small open circles.

Table II. Characteristics of Ginger's eye on September 25, 1971. Eye types a through f are defined in the text. C, wall-cloud diameter in nm, $\bar{C}$ mean wall-cloud diameter, E, equivalent eye diameter in nm, $\bar{E}$, mean equivalent eye diameter, $\bar{E}/\bar{C}$, eye index, P_c smoothed central pressure, and $\bar{P}_c$, estimated central pressure.

ATS Frame	Time GMT	Eye Type	C	$\bar{C}$	E	$\bar{E}$	$\bar{E}/\bar{C}$	P_c	$\bar{P}_c$
1	1202	c	70	--	30	--	--	978	---
2	1229	c	70	--	40	--	--	978	---
3	1255	d	80	72	30	28	0.39	978	978
4	1322	e	70	74	20	26	0.35	978	979
5	1349	e	70	76	20	22	0.29	978	980
6	1416	e	80	72	20	22	0.30	977	979
7	1443	e	80	67	20	25	0.37	977	978
8	1510	d	60	63	30	27	0.43	977	976
9	1522	d	60	60	30	29	0.48	977	976
10	1538	c	50	60	30	29	0.48	977	976
11	1544	c	50	58	30	30	0.52	977	974
12	1604	c	60	58	30	30	0.52	977	974
13	1616	b	60	58	30	30	0.52	977	974
14	1631	b	60	56	30	30	0.54	976	974
15	1642	b	60	56	30	30	0.54	976	974
16	1654	b	60	56	30	30	0.54	976	974
17	1709	-	--	--	--	--	--	976	---
18	1724	b	50	55	30	33	0.60	976	972
19	1735	b	50	56	30	35	0.62	976	972
20	1750	b	50	56	30	36	0.64	976	972
21	1802	c	50	56	40	36	0.64	976	972
22	1817	b	60	57	40	36	0.63	976	972
23	1829	d	70	58	50	34	0.59	976	973
24	1848	c	60	59	40	33	0.56	976	974
25	1856	d	60	60	30	32	0.53	976	974
26	1911	d	60	61	30	30	0.49	975	975
27A	1922	e	60	61	20	28	0.46	975	976
27B	1937	e	60	60	20	26	0.43	975	976
28	1949	e	60	61	20	24	0.39	975	977
29	2005	d	60	61	20	24	0.39	975	977
30	2015	d	60	--	20	--	--	975	---
31	2031	c	60	--	30	--	--	975	---
32	2042	c	70	--	30	--	--	975	---
33	2109	-	--	--	--	--	--	975	---
34	2122	Dark						975	
35	2137	Dark						975	
36	2148	Dark						975	
37	2203	Very Dark						975	
38	2215	Not Visible						975	

Table III. Characteristics of Ginger's eye on September 26, 1971. Eye types a through f are defined in the text. C, wall-cloud diameter in nm, $\bar{C}$ mean wall-cloud diameter, E, equivalent eye diameter in nm, $\bar{E}$, mean equivalent eye diameter, $\bar{E}/\bar{C}$, eye index, P_c smoothed central pressure, and $\bar{P}_c$, estimated central pressure.

ATS Frame	Time GMT	Eye Type	C	$\bar{C}$	E	$\bar{E}$	$\bar{E}/\bar{C}$	P_c	$\bar{P}_c$
1	1208	d	80	--	40	--	--	982	---
2	1235	d	70	75	30	32	0.43	982	978
3	1301	d	70	76	30	32	0.42	983	978
4	1329	d	80	78	30	30	0.38	983	979
5	1356	d	80	82	30	30	0.37	983	980
6	1423	d	90	88	30	32	0.36	983	980
7	1449	d	90	97	30	38	0.39	983	981
8	1516	d	100	100	40	43	0.43	984	981
9	1529	d	110	101	50	47	0.47	984	981
10	1543	d	110	100	50	48	0.48	984	981
11	1554	e	100	98	50	48	0.49	984	980
12	1609	e	100	97	50	49	0.51	984	980
13	1621	e	100	97	60	48	0.50	984	980
14	1635	e	90	96	50	44	0.46	983	980
15	1647	e	80	94	50	42	0.45	983	980
16	1702	e	80	96	40	40	0.42	983	981
17	1713	e	100	96	30	39	0.40	983	981
18	1729	e	100	95	20	36	0.38	983	981
19	1740	e	100	96	30	33	0.34	983	982
20	1756	e	110	96	30	37	0.39	983	981
21	1803	e	100	94	40	30	0.32	982	982
22	1822	e	100	91	30	29	0.32	982	981
23	1833	e	90	89	30	29	0.33	982	981
24	1849	d	80	87	40	28	0.32	981	981
25	1900	e	70	83	20	27	0.33	981	980
26	1916	e	70	84	20	24	0.29	981	981
27	1926	e	80	81	20	23	0.29	980	980
28	1939	d	80	82	20	22	0.27	980	981
29	1951	d	80	86	20	20	0.23	980	982
30	2006	d	90	86	20	20	0.23	980	982
31	2016	e	90	--	20	--	--	980	---
32	2032	e	100	--	20	--	--	980	---
33	2042	e	100	--	20	--	--	980	---
34	2109	dark						980	
35	2127	dark						980	
36	2137	very dark						980	
37	2148	very dark						980	
38	2204	not visible						980	
39	2216	not visible						980	

Table IV. Characteristics of Ginger's eye on September 27, 1971. Eye types a through f are defined in the text. C, wall-cloud diameter in nm, $\bar{C}$, mean wall-cloud diameter, E, equivalent eye diameter in nm, $\bar{E}$, mean equivalent eye diameter, $\bar{E}/\bar{C}$, eye index, P_c smoothed central pressure, and $\bar{P}_c$, estimated central pressure.

ATS Frame	Time GMT	Eye Type	C	$\bar{C}$	E	$\bar{E}$	$\bar{E}/\bar{C}$	P_c	$\bar{P}_c$
1	1248	c	60	--	50	--	--	973	---
2	1315	d	60	--	40	--	--	973	---
3	1342	c	60	60	50	46	0.77	973	970
4	1409	c	60	60	50	44	0.74	972	970
5	1436	c	60	60	40	44	0.74	972	970
6	1503	c	60	60	40	42	0.70	972	971
7	1530	c	60	60	40	40	0.66	971	972
8	1557	c	60	59	40	40	0.68	971	971
9	--	-	--	--	--	--	--	970	---
10	1623	c	60	60	40	40	0.66	970	972
11	1635	c	50	60	40	40	0.66	970	972
12	1650	b	60	59	40	38	0.64	970	972
13	1702	c	60	59	40	38	0.64	970	972
14	1717	c	70	58	40	38	0.66	970	972
15	1729	c	60	58	40	37	0.64	969	972
16	1744	d	60	61	30	36	0.59	969	973
17	1755	c	50	59	30	34	0.58	969	972
18	1811	b	50	59	40	34	0.58	969	973
19	1822	b	60	59	30	38	0.64	969	972
20	1837	c	60	60	30	34	0.58	969	973
21	1849	c	60	60	30	36	0.60	969	973
22	1904	c	60	62	40	41	0.66	969	972
23	1915	c	70	64	40	42	0.66	969	973
24	1931	c	70	64	40	40	0.62	968	974
25	1942	d	60	64	40	41	0.64	968	973
26	1958	c	70	64	50	43	0.67	968	972
27	2009	b	70	64	50	43	0.67	968	972
28	2025	c	60	63	40	43	0.67	968	972
29	2036	b	60	62	40	43	0.69	968	972
30	2047	b	60	62	50	44	0.71	968	971
31	2057	b	60	--	40	--	--	968	---
32	2113	c	60	--	40	--	--	968	---
33	2124	b	60	--	40	--	--	968	---
34	2140	dark						968	
35	2151	dark						968	
36	2207	very dark						969	
37	2218	not visible						969	

Table V. Characteristics of Ginger's eye on September 28, 1971. Eye types a through f are defined in the text. C, wall-cloud diameter in nm, $\bar{C}$, mean wall-cloud diameter, E, equivalent eye diameter in nm, $\bar{E}$, mean equivalent eye diameter, $\bar{E}/\bar{C}$, eye index, P_c smoothed central pressure, and $\bar{P}_c$, estimated central pressure.

ATS Frame	Time GMT	Eye Type	C	$\bar{C}$	E	$\bar{E}$	$\bar{E}/\bar{C}$	P_c	$\bar{P}_c$
1	1230	d	120	---	40	--	--	982	---
2	1257	c	120	---	40	--	--	982	---
3	1324	d	110	112	30	32	0.29	982	983
4	1350	d	100	112	20	32	0.29	982	983
5	1417	c	110	110	30	32	0.29	982	983
6	1444	d	120	108	40	32	0.30	982	983
7	1511	d	110	106	40	34	0.32	982	982
8	1538	c	100	101	30	35	0.35	982	982
9	1550	d	90	98	30	35	0.36	982	982
10	--	-	---	---	--	--	--	982	---
11	1617	d	100	93	30	33	0.36	981	981
12	1632	d	90	95	40	34	0.36	981	981
13	1643	d	90	95	40	35	0.37	981	981
14	1659	c	80	98	30	35	0.36	981	982
15	1710	c	100	98	30	35	0.36	981	982
16	1726	c	110	99	40	37	0.37	981	982
17	1737	c	100	100	40	41	0.41	980	981
18	1752	d	110	101	30	45	0.44	980	981
19	1803	-	---	---	--	--	--	980	---
20	1819	d	110	104	50	52	0.50	980	981
21	1829	d	100	104	70	55	0.53	980	980
22	1845	e	90	106	70	56	0.53	980	980
23	1856	d	100	106	60	59	0.56	980	980
24	1913	d	110	106	60	59	0.56	980	980
25	1925	d	110	106	60	61	0.58	980	980
26	1938	c	110	108	50	60	0.55	980	981
27	1949	c	110	110	50	60	0.55	980	981
28	2005	d	110	111	60	61	0.55	980	981
29	2017	d	110	113	70	62	0.55	980	981
30	2032	c	110	114	60	62	0.54	980	981
31	2044	d	120	118	70	66	0.56	980	982
32	2059	d	110	121	70	70	0.58	980	982
33	2116	d	130	---	70	--	--	980	---
34	2137	e	140	---	80	--	--	981	---
35	2156	e	140	---	80	--	--	982	---

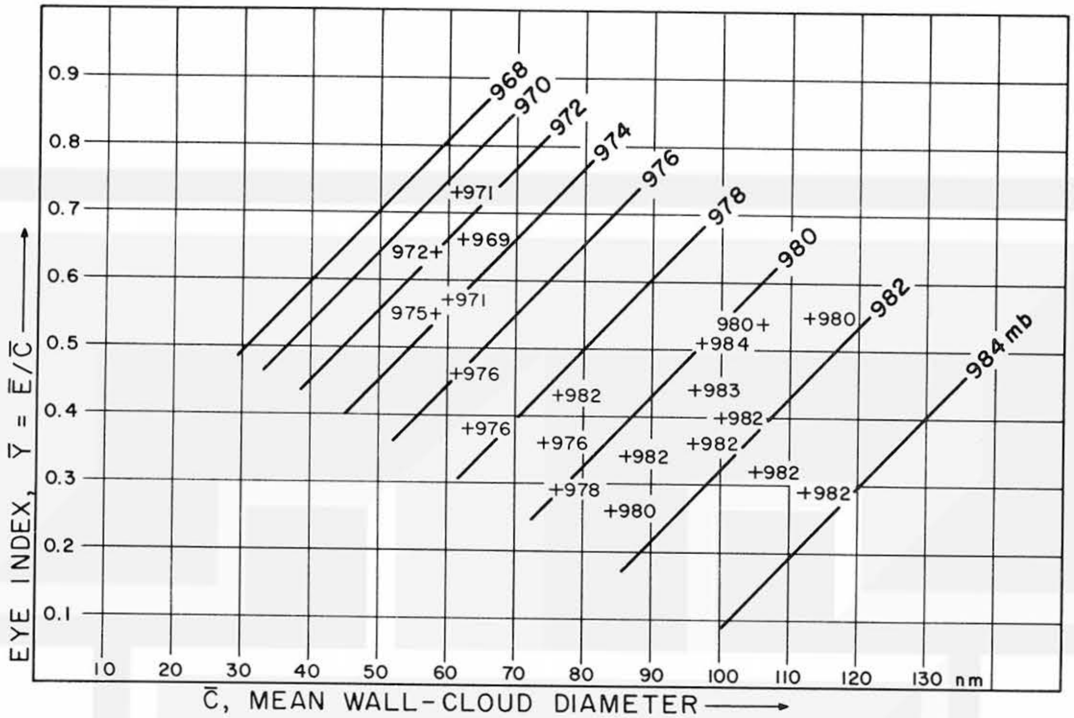

Figure 8. Central pressure of Ginger plotted as a function of eye index and mean wall-cloud diameter.

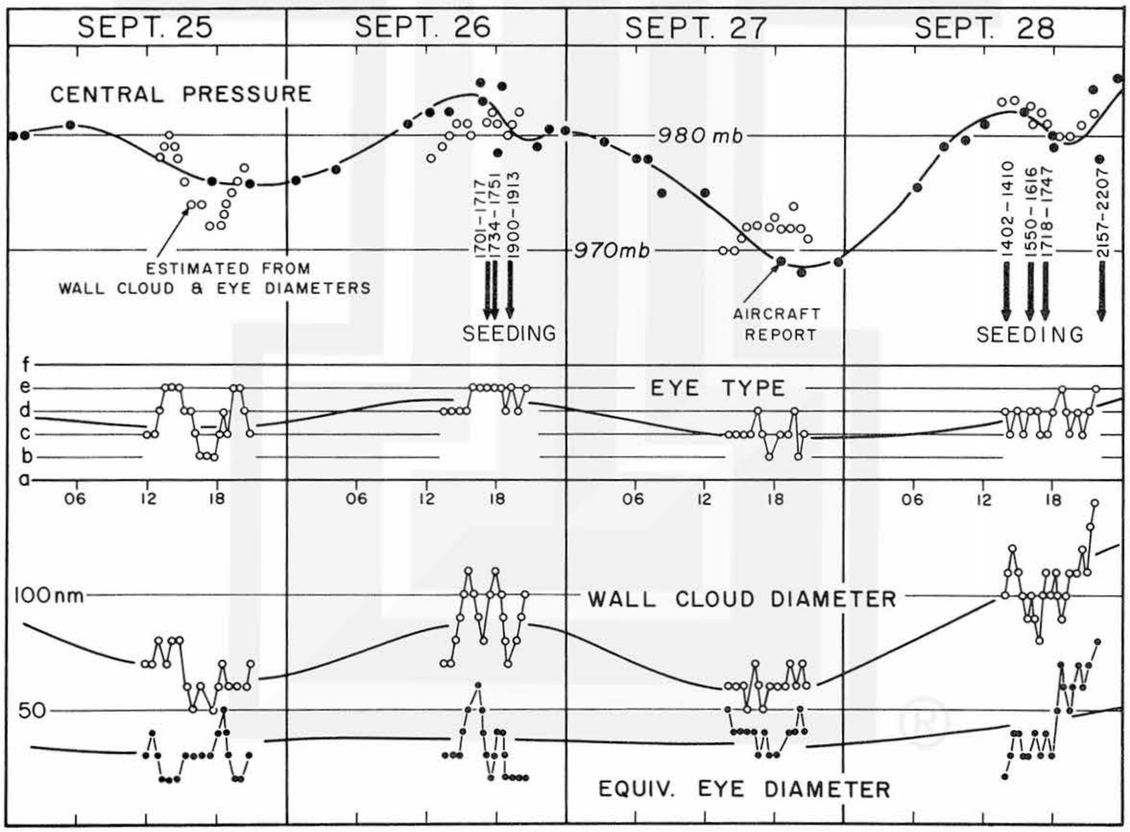

Figure 9. Variation of Ginger's eye parameters during a 4-day period, Sept. 25 through 28.

5. TIME INTEGRATION OF ATS PICTURES

To explore possible means of using ATS pictures for detection of variations in overall cloud patterns of a seeded hurricane, several ATS pictures were put together into a "composite" or "time-integrated" picture. Such a time integration will smooth out fast-moving and fast-developing nephsystems while conserving the overall patterns lasting at least during the integration period.

Time integration of pictures can be performed with or without weighting function which can be designed to put more weight on specified pictures. Results of a test of 5-picture integration are presented in Fig. 10. Each of the three pictures was produced through a multiple exposure of 5 negatives onto a photographic paper. The total exposure time was kept constant to be 10 second, however, the exposure time of each negative was changed as follows

Negatives	A	B	C	D	E	Total
Top picture	2 sec	2 sec	2 sec	2 sec	2 sec	10 sec
Middle picture	3 sec	3 sec	2 sec	1 sec	1 sec	10 sec
Bottom picture	4 sec	2 sec	2 sec	1 sec	1 sec	10 sec

In exposing the negatives, the positions of the hurricane center were kept at a constant location on the photographic paper to allow a time integration relative to the hurricane eye. Against expectation that a weighting will result in significant differences in the appearance of the storm, three test pictures, thus produced, turned out to be very similar to each other. Similar tests made with a series of other negatives ended up with practically the same results, suggesting that weighted exposures for time integration are not worthwhile in view of time consumption vs effectiveness.

To determine the day-to-day variations of Ginger between September 25 and 28, all available pictures on each day were integrated into one picture. The results of the daily time integration are presented in Fig. 11. Photographs include local longitude and latitude through the center of the eye. Short markers on both latitude and longitude are placed for every 100 nautical miles measured from the eye center.

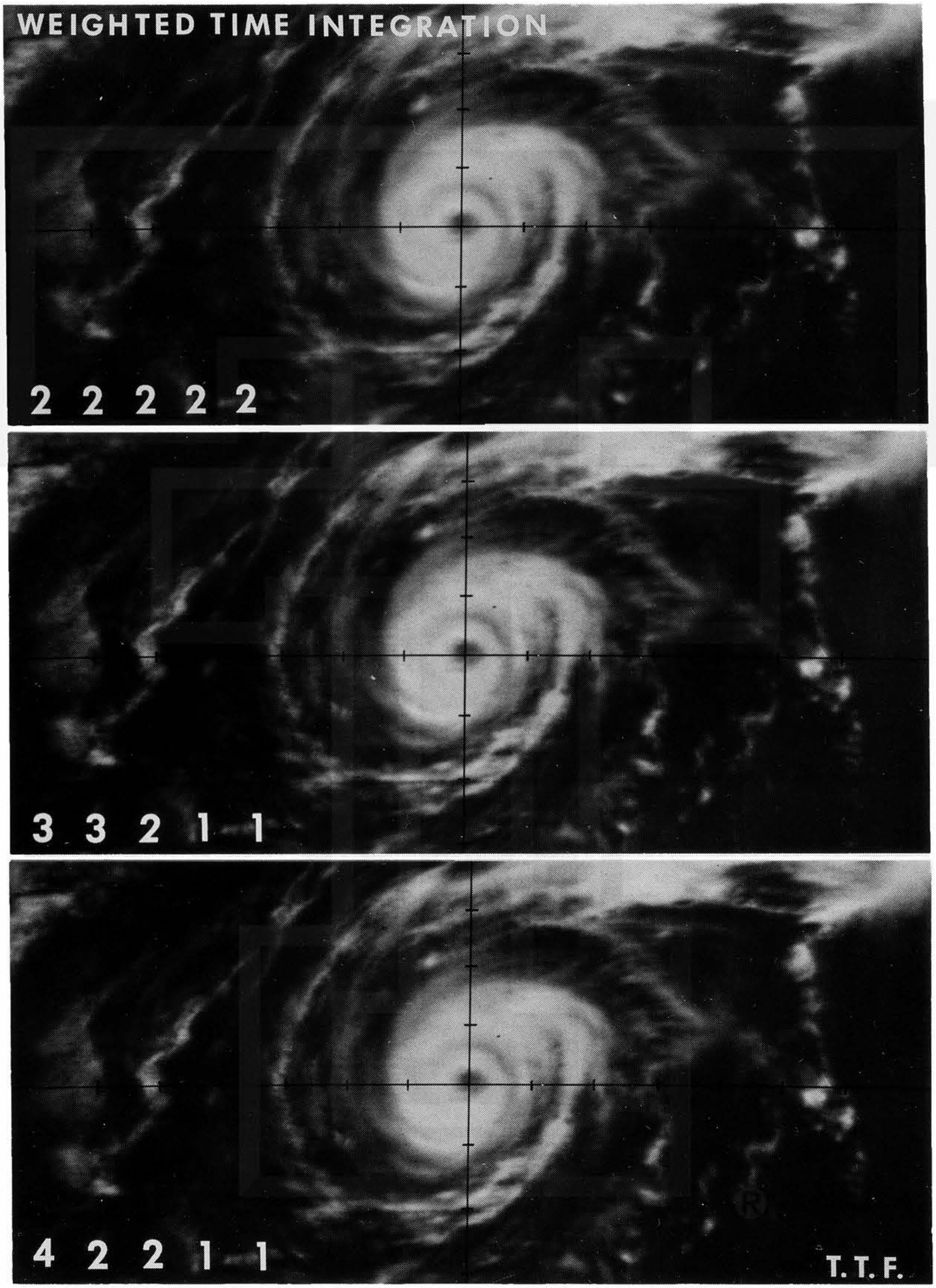

Figure 10. Weighted time integration of ATS III picture showing Ginger.

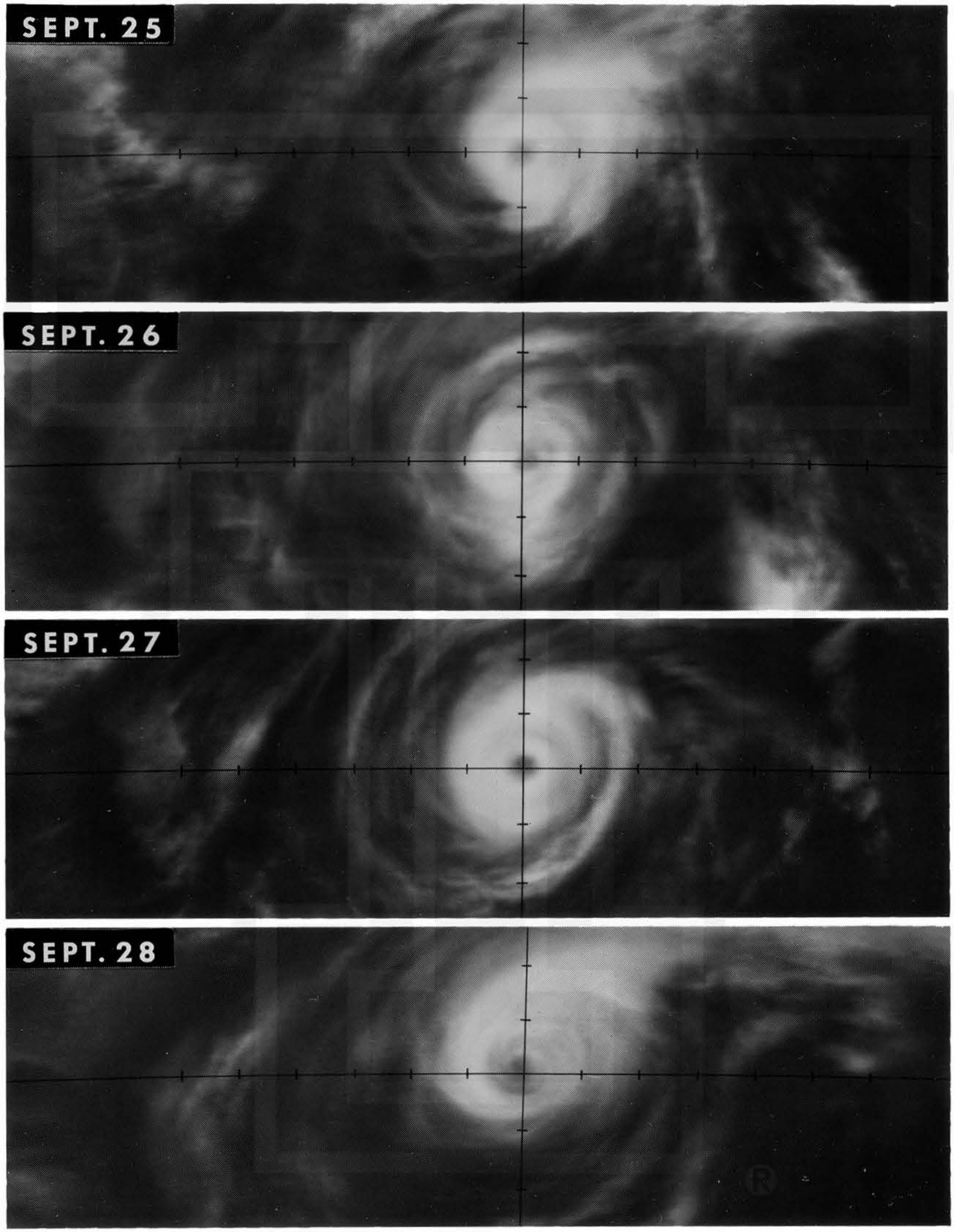

Figure 11. Daily time integration of Ginger. Seeding experiments were conducted on Sept. 26 and 28.

Due to the movement of the hurricane, the position of Florida seen near the left edge of the September 25 picture moved to the right as the day progressed to September 28. The eye was the smallest and the darkest on September 27 when the central pressure was the lowest within this 4-day period. The overall cloud patterns were more or less axially symmetric on September 26. On other days, northeast expansion of extensive clouds was apparent.

In order to visualize cloud variation within each day of sun-lit hours, the photographic period within each day was divided into three periods. Then the pictures available within each period were integrated into one picture, thus producing a set of three pictures each day.

Results from September 25 pictures divided into 1202-1604, 1616-1817, and 1829-2042 are presented in Fig. 12. No seeding was performed on this day. Any change appearing in this picture sequence should be regarded as natural variations.

The three pictures in Fig. 13 were made by integrating September 26 pictures taken between 1423-1647, 1702-1849, and 1900-2042. No seeding was performed within the first period, but the second period includes 1701-1717 and 1734-1751 seedings. The last period includes 1900-1913 seeding. The locations of these seedings are indicated by the series of black dots superimposed upon the time-integrated pictures.

September 27 was a day of no seeding. Time integration was performed for three periods, 1409-1635, 1650-1837, and 1837-2009. The change in the cloud pattern on this day within the area of the storm was minor, showing a slight rotation of nephsystems around the eye. Within the immediate vicinity of the eye, very little variation in the integrated cloud patterns is seen in the tangential direction due to relatively fast rotational cloud motions. It should be noted, however, that there is a dark concentric circle with 70 to 80 nm radius surrounding the eyewall clouds. This feature might imply that the storm on the 27th was axially symmetric within some 100 nm from the center.

Three-time integrated pictures of September 28 divided into 1350-1710, 1726-1925, and 1938-2156 periods are presented in Fig. 15. Most locations of seeding are seen in the northeast sector of the storm where intense rainbands are entering the central

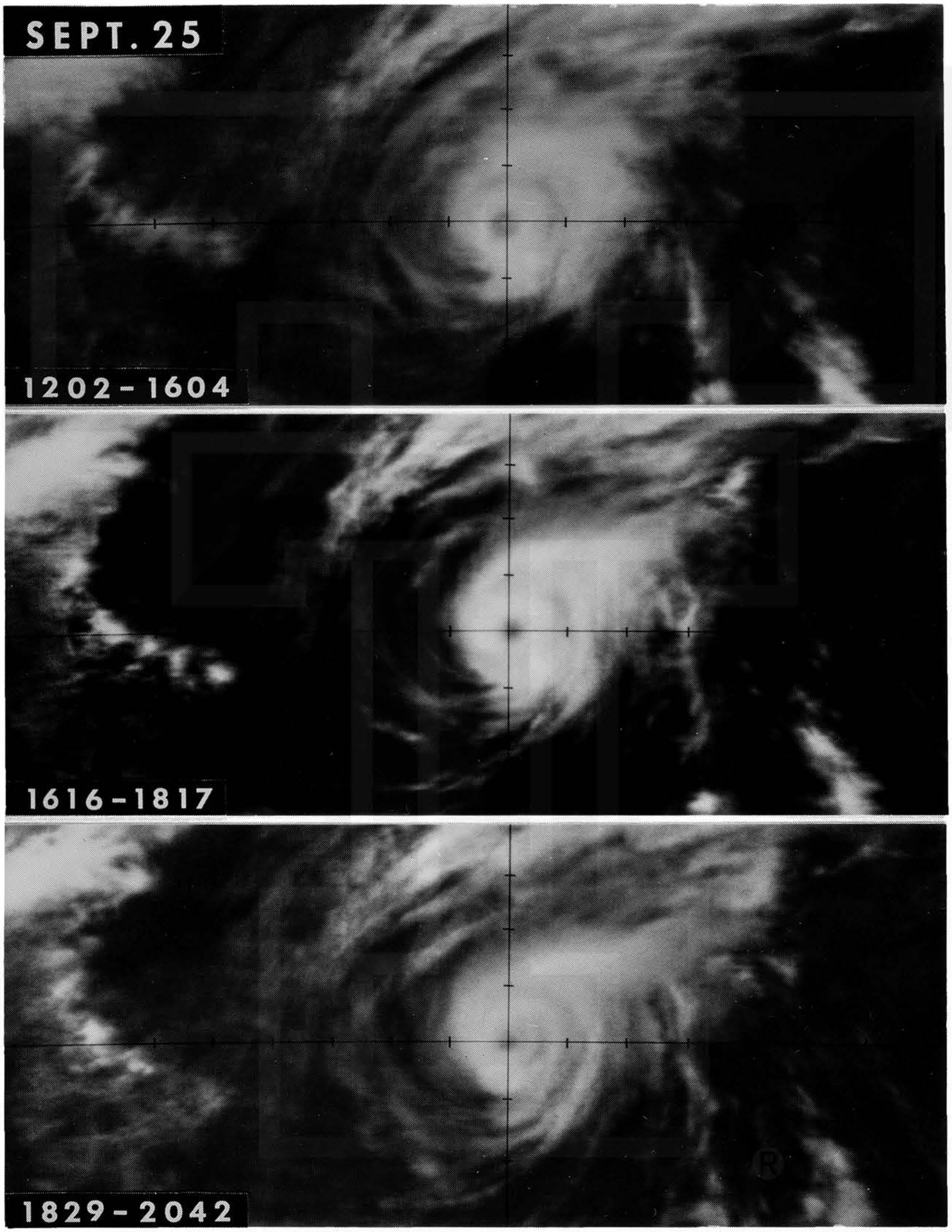

Figure 12. Time integration of Ginger pictures on Sept. 25, 1971.

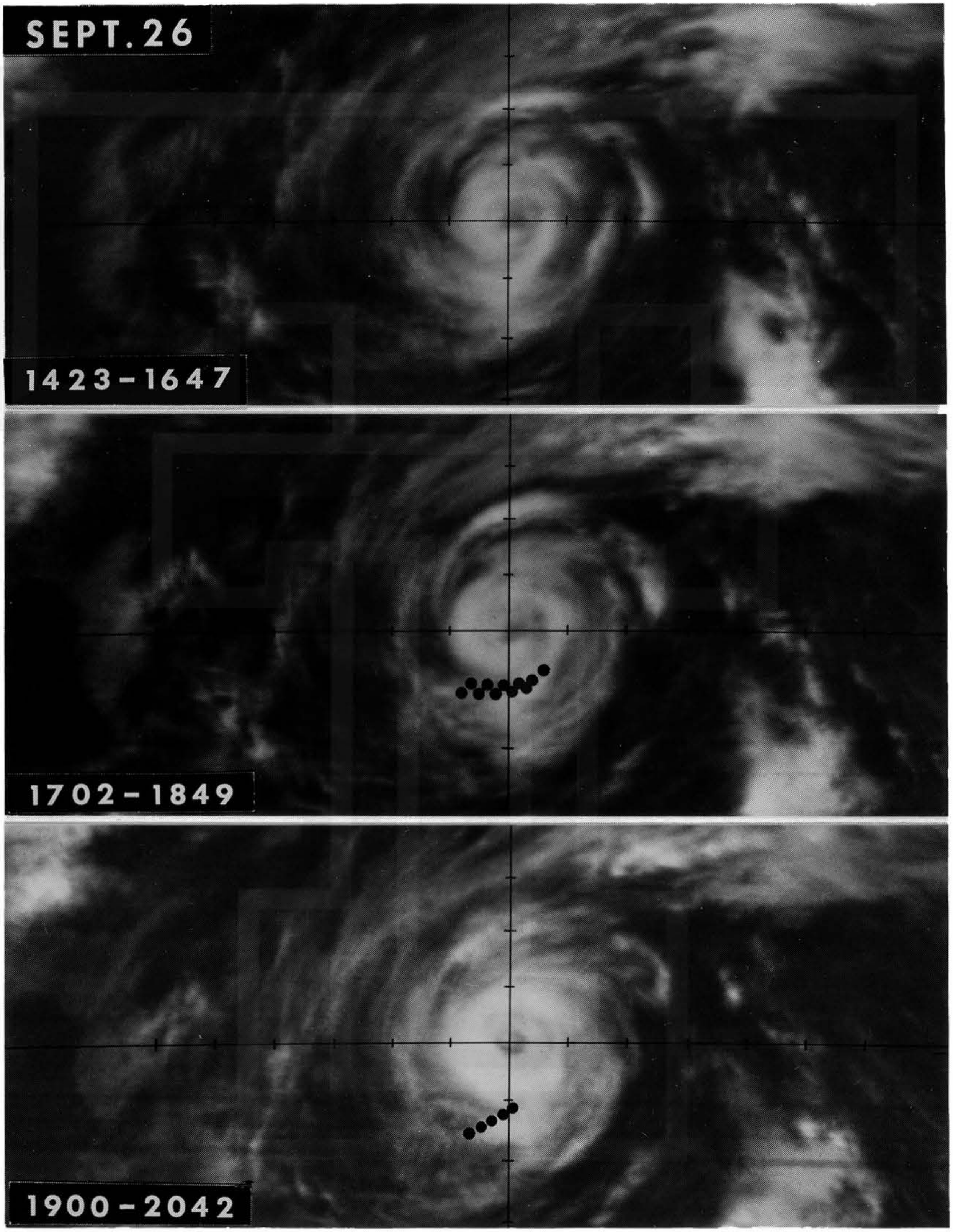

Figure 13. Time integration of Ginger pictures on Sept. 26, 1971.

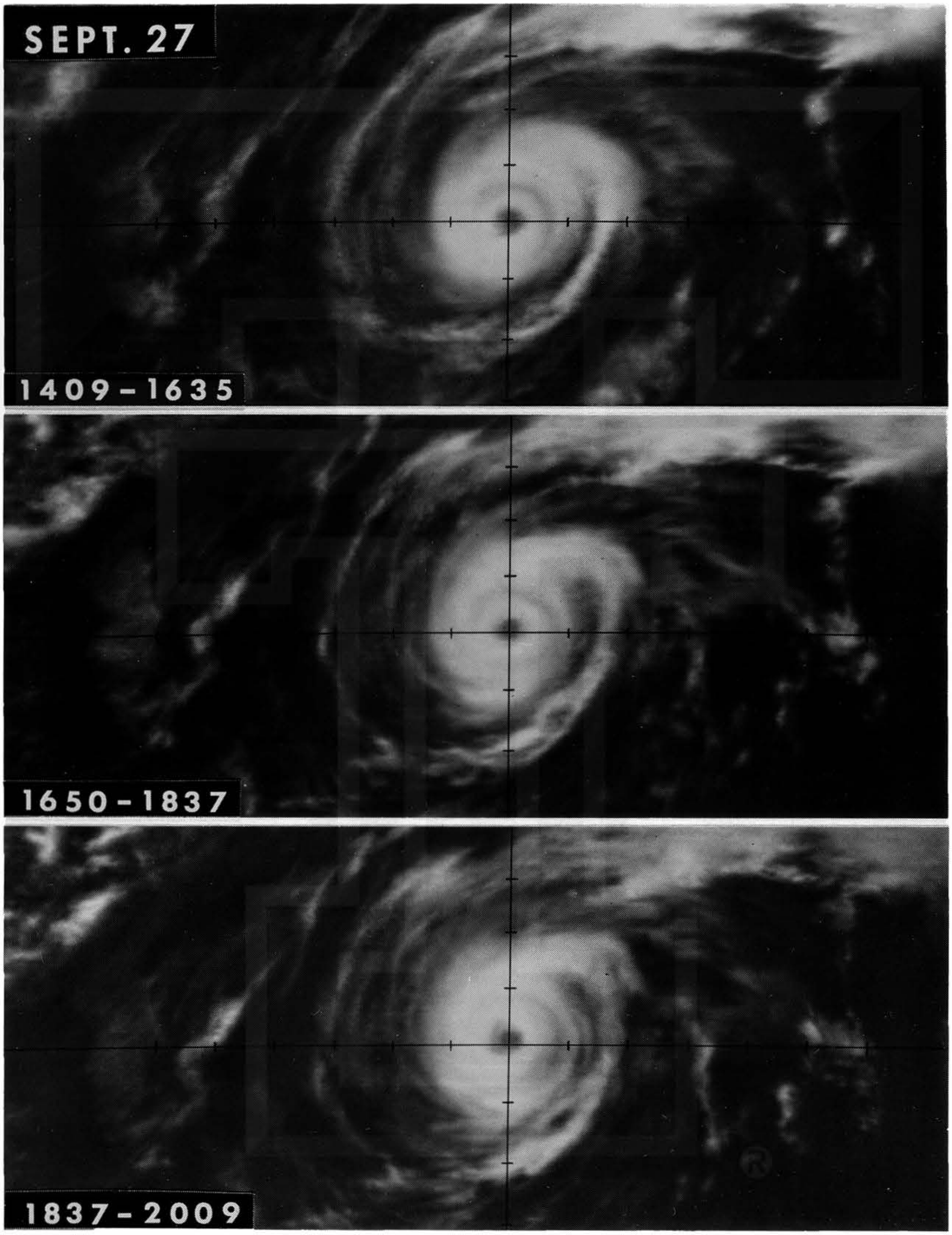

Figure 14. Time integration of Ginger pictures on Sept. 27, 1971.

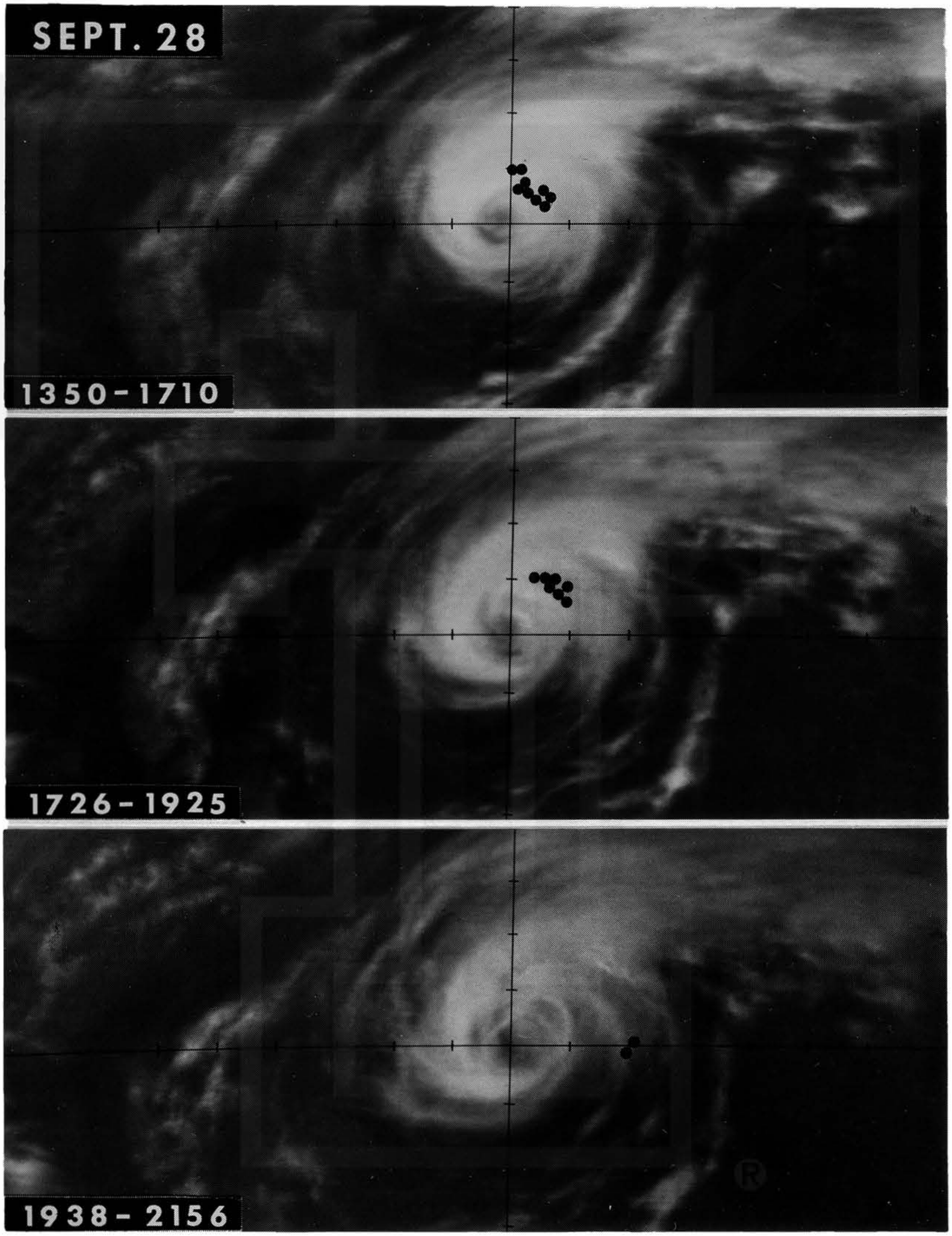

Figure 15. Time integration of Ginger pictures on Sept. 28, 1971.

region of the storm. Of interest is the significant expansion of the eye wall seen in the last picture. The picture gives an impression that the eyewall circulation is falling apart.

Presented here is a four-day sequence of 4 x 3 = 12 pictures, each of which was produced by integrating several pictures taken within one-third of the sun-lit period of each day. This sequence is supposed to show the effects of modification if they are significant enough and distinguishable from natural variations. In order not to create misunderstanding in the judgment of natural vs. artificial changes in hurricane structure as seen from ATS, the author wishes to leave such judgments up to the readers. Undoubtedly, there are variations between successive pictures in this sequence. However, it is very difficult to determine the extent of natural variations which are likely to obscure artificial variations.

To further assist the evaluation of hurricane modification, a 90-ft movie on 16-mm film was produced as an Appendix. For further detail, refer to the Appendix.

6. CONCLUSIONS

Results of this study revealed that the changes in cloud patterns expected from the modification hypotheses are to be detected from sequences of ATS pictures. First of all, the increase in the vertical motion, due to the release of the latent heat of fusion which varies between 80 to 50 cal/g as the freezing temperature decreases from 0 to -50C, should be observed as a rapid expansion of the tops of convective towers. Convective warming thus created will reduce the pressure gradient beneath the towers resulting ultimately in the expansion of the eyewall. When the additional buoyancy generated by the heat of fusion stimulates the inflow, chain reaction as predicted by modification hypotheses will rapidly increase the apparent eye diameter. Meanwhile, the outflow field will be accelerated. Note that Hawkins et al (1972) discussed the changes that should be expected in hurricane Ginger following the modification experiments.

There is no reason to believe that such a change in the cloud patterns cannot be recognized in successive ATS pictures with 2 to 3 mile resolution. Recognition of expected variations can be improved by means of improved methods of ATS picture analyses such as time-lapse technique, time-integrated pictures, special pattern recognition etc.

A serious problem which will be with us for years to come is the separation of man-made changes from natural variations. Such a separation is possible only when modification effects are more significant than natural variations or somewhat different from nature's behavior.

It is necessary, therefore, that ATS pictures be investigated for a period much longer than the modification period. Frequent pictures and digital tapes must be made for a seven-day period so that an analysis of the storm's natural variations can be investigated in detail beginning two days prior to and ending two days after the modification period.

Meanwhile, a careful and organized aerial photogrammetric survey of a hurricane under modification would be highly desirable. Such an experiment conducted simultaneously with seeding experiment will be an important cloud truth experiment.

REFERENCES

Black, P. G. (1971): Use of Echo Velocities to evaluate Hurricane Modification Experiment. Appendix J, Annual Report of 1970 Project Stormfury.

Hawkins, H. F., K. H. Bergman, and R. C. Gentry (1972): Report on Seeding of Hurricane Ginger. Appendix B, Annual Report of 1971 Project Stormfury.

Project Stormfury (1971): Annual Report of 1970 Project Stormfury. NHRL and Naval Weather Service.

Simpson, R. H. and J. R. Hope (1972): Atlantic Hurricane Season of 1971. Mon. Wea. Rev. Vol. 100, pp. 256-267.

APPENDIX

A motion picture entitled "Hurricane Ginger of September 1971" was produced as an Appendix to SMRP Research Paper No. 106. A copy of this film can be obtained either from

Dr. R. Cecil Gentry
National Hurricane Research Laboratory
P. O. Box 8265
Coral Gables, Florida 33124

or

Professor T. Theodore Fujita
Department of Geophysical Sciences
University of Chicago
Chicago, Illinois 60637

Description of this 90-ft movie is presented hereunder.

The movie begins with the titles "Hurricane Ginger September 1971", "ATS III Views of Stormfury Experiment directed by R. Cecil Gentry" and "Produced by T. Theodore Fujita". The movie covers a 4-day period, September 25-28. Time-lapse movie for each day was produced from (1) Individual ATS pictures and (2) Time-integrated pictures consisting of a composite of 5 pictures, such as 1 through 5, 2 through 6, 3 through 7, etc. These sequences are identified as single-image movie and time-integrated movie, respectively.

September 25 (day before seeding) was filmed from 30 individual pictures taken between 1202 and 2042 GMT. The first picture was filmed 20 times followed by successive pictures filmed 2 frames each. One cycle, thus, consisting of 68 frames was repeated five times to show the evolution of the storm on the 25th. The second portion of the film on September 25 was made from 25 time-integrated pictures each consisting of 5 successive pictures. A 5-cycle sequence was filmed using the identical filming schedule to that applied to the single-image movie.

September 26 (day of seeding) was filmed from 29 individual pictures taken between 1235 and 2042 GMT. From these pictures, a sequence of 24 time-integrated pictures were made to produce a 5-cycle film of the single-image and time-integrated movie. Locations of seedings are identified by small red dots superimposed upon ATS pictures nearest to the seeding time. When the film is viewed at the normal projection speed red dots on a moving-cloud image reveals Stormfury's seeding activities.

September 27 (day between seedings) was filmed from 23 individual pictures taken between 1409 and 2009 GMT. A sequence of 18 time-integrated pictures was used in filming the time-integrated movie of this day.

September 28 (day of seeding) was filmed from 30 individual pictures taken between 1350 and 2156 GMT. 25 time-integrated pictures were made from these pictures. As in the case of the 26th, seeding locations are identified with red dots appearing on images of moving clouds.

It is seen in the movie that the cloud motion on the single-image movie is relatively fast as expected. The time-integrated movie, however, is not sensitive to the motion of individual clouds, but it shows the group motions of individual clouds undergoing development or decay. Repeated examination of this time lapse movie of Ginger will assist further evaluation of the seeding effects if they are significant enough to affect ATS-viewed nephsystems and are 2 to 3 nautical miles or larger in horizontal dimensions.

This film was produced at SMRP of the University of Chicago under the sponsorship of NHRL grant N 22-21-72 (G). Photographic work of NOAA negatives was supported by NESS under grant E-198-68 (G), and 4X and high-quality enlargement, by NASA under grant NGR 14-001-008. Without these supports, this movie could not have been completed.

MESOMETEOROLOGY PROJECT - - - RESEARCH PAPERS

(Continued from front cover)

42.* A Study of Factors Contributing to Dissipation of Energy in a Developing Cumulonimbus - Rodger A. Brown and Tetsuya Fujita

43. A Program for Computer Gridding of Satellite Photographs for Mesoscale Research - William D. Bonner

44. Comparison of Grassland Surface Temperatures Measured by TIROS VII and Airborne Radiometers under Clear Sky and Cirriform Cloud Conditions - Ronald M. Reap

45. Death Valley Temperature Analysis Utilizing Nimbus I Infrared Data and Ground-Based Measurements - Ronald M. Reap and Tetsuya Fujita

46. On the "Thunderstorm-High Controversy" - Rodger A. Brown

47. Application of Precise Fujita Method on Nimbus I Photo Gridding - Lt. Cmd. Ruben Nasta

48. A Proposed Method of Estimating Cloud-top Temperature, Cloud Cover, and Emissivity and Whiteness of Clouds from Short- and Long-wave Radiation Data Obtained by TIROS Scanning Radiometers - T. Fujita and H. Grandoso

49. Aerial Survey of the Palm Sunday Tornadoes of April 11, 1965 - Tetsuya Fujita

50. Early Stage of Tornado Development as Revealed by Satellite Photographs - Tetsuya Fujita

51. Features and Motions of Radar Echoes on Palm Sunday, 1965 - D. L. Bradbury and T. Fujita

52. Stability and Differential Advection Associated with Tornado Development - Tetsuya Fujita and Dorothy L. Bradbury

53. Estimated Wind Speeds of the Palm Sunday Tornadoes - Tetsuya Fujita

54. On the Determination of Exchange Coefficients: Part II - Rotating and Nonrotating Convective Currents - Rodger A. Brown

55. Satellite Meteorological Study of Evaporation and Cloud Formation over the Western Pacific under the Influence of the Winter Monsoon - K. Tsuchiya and T. Fujita

56. A Proposed Mechanism of Snowstorm Mesojet over Japan under the Influence of the Winter Monsoon - T. Fujita and K. Tsuchiya

57. Some Effects of Lake Michigan upon Squall Lines and Summertime Convection - Walter A. Lyons

58. Angular Dependence of Reflection from Stratiform Clouds as Measured by TIROS IV Scanning Radiometers - A. Rabbe

59. Use of Wet-beam Doppler Winds in the Determination of the Vertical Velocity of Raindrops inside Hurricane Rainbands - T. Fujita, P. Black and A. Loesch

60. A Model of Typhoons Accompanied by Inner and Outer Rainbands - Tetsuya Fujita, Tatsuo Izawa., Kazuo Watanabe and Ichiro Imai

*61. Three-Dimensional Growth Characteristics of an Orographic Thunderstorm System - Rodger A. Brown

62. Split of a Thunderstorm into Anticyclonic and Cyclonic Storms and their Motion as Determined from Numerical Model Experiments - Tetsuya Fujita and Hector Grandoso

63. Preliminary Investigation of Peripheral Subsidence Associated with Hurricane Outflow - Ronald M. Reap

64. The Time Change of Cloud Features in Hurricane Anna, 1961, from the Easterly Wave Stage to Hurricane Dissipation - James E. Arnold

65. Easterly Wave Activity over Africa and in the Atlantic with a Note on the Intertropical Convergence Zone during Early July 1961 - James E. Arnold

66. Mesoscale Motions in Oceanic Stratus as Revealed by Satellite Data - Walter A. Lyons and Tetsuya Fujita

67. Mesoscale Aspects of Orographic Influences on Flow and Precipitation Patterns - Tetsuya Fujita

68. A Mesometeorological Study of a Subtropical Mesocyclone -Hidetoshi Arakawa, Kazuo Watanabe, Kiyoshi Tsuchiya and Tetsuya Fujita

69. Estimation of Tornado Wind Speed from Characteristic Ground Marks - Tetsuya Fujita, Dorothy L. Bradbury and Peter G. Black

70. Computation of Height and Velocity of Clouds from Dual, Whole-Sky, Time-Lapse Picture Sequences - Dorothy L. Bradbury and Tetsuya Fujita

71. A Study of Mesoscale Cloud Motions Computed from ATS-I and Terrestrial Photographs - Tetsuya Fujita, Dorothy L. Bradbury, Clifford Murino and Louis Hull

72. Aerial Measurement of Radiation Temperatures over Mt. Fuji and Tokyo Areas and Their Application to the Determination of Ground- and Water-Surface Temperatures - Tetsuya Fujita, Gisela Baralt and Kiyoshi Tsuchiya

73. Angular Dependence of Reflected Solar Radiation from Sahara Measured by TIROS VII in a Torquing Maneuver - Rene Mendez.

74. The Control of Summertime Cumuli and Thunderstorms by Lake Michigan During Non-Lake Breeze Conditions - Walter A. Lyons and John W. Wilson

75. Heavy Snow in the Chicago Area as Revealed by Satellite Pictures - James Bunting and Donna Lamb

76. A Model of Typhoons with Outflow and Subsidence Layers - Tatsuo Izawa

* out of print

(continued on outside back cover)

SATELLITE AND MESOMETEOROLOGY RESEARCH PROJECT --- PAPERS
(Continued from inside back cover)

77. Yaw Corrections for Accurate Gridding of Nimbus HRIR Data - Roland A. Madden

78. Formation and Structure of Equatorial Anticyclones Caused by Large-Scale Cross Equatorial Flows Determined by ATS I Photographs - Tetsuya T. Fujita and Kazuo Watanabe and Tatsuo Izawa.

79. Determination of Mass Outflow from a Thunderstorm Complex Using ATS III Pictures - T. T. Fujita and D. L. Bradbury.

80. Development of a Dry Line as Shown by ATS Cloud Photography and Verified by Radar and Conventional Aerological Data - Dorothy L. Bradbury.

81. Dynamical Analysis of Outflow from Tornado-Producing Thunderstorms as Revealed by ATS III Pictures - K. Ninomiya.

82.** Computation of Cloud Heights from Shadow Positions through Single Image Photogrammetry of Apollo Pictures - T. T. Fujita.

83. Aircraft, Spacecraft, Satellite and Radar Observations of Hurricane Gladys, 1968 - R. Cecil Gentry, Tetsuya T. Fujita and Robert C. Sheets.

84. Basic Problems on Cloud Identification Related to the Design of SMS-GOES Spin Scan Radiometers - Tetsuya T. Fujita.

85. Mesoscale Modification of Synoptic Situations over the Area of Thunderstorms' Development as Revealed by ATS III and Aerological Data - K. Ninomiya.

86. Palm Sunday Tornadoes of April 11, 1965 - T. T. Fujita, Dorothy L. Bradbury and C. F. Van Thullenar (Reprint from Mon. Wea. Rev., 98, 29-69, 1970).

87. Patterns of Equivalent Blackbody Temperature and Reflectance of Model Clouds Computed by Changing Radiometer's Field of View - Jaime J. Tecson.

88. Lubbock Tornadoes of 11 May 1970 - Tetsuya Theodore Fujita.

89. Estimate of Areal Probability of Tornadoes from Inflationary Reporting of Their Frequencies - Tetsuya T. Fujita.

90. Application of ATS III Photographs for Determination of Dust and Cloud Velocities Over Northern Tropical Atlantic - Tetsuya T. Fujita.

91. A Proposed Characterization of Tornadoes and Hurricanes by Area and Intensity - Tetsuya T. Fujita.

92. Estimate of Maximum Wind Speeds of Tornadoes in Three Northwestern States - T. Theodore Fujita.

93. In- and Outflow Field of Hurricane Debbie as Revealed by Echo and Cloud Velocities from Airborne Radar and ATS-III Pictures - T. T. Fujita and P. G. Black (Reprinted from preprint of Radar Meteorology Conference, November 17-20, 1970, Tucson, Arizona).

94.** Characterization of 1965 Tornadoes by their Area and Intensity - Jaime J. Tecson.

95.* Computation of Height and Velocity of Clouds over Barbados from a Whole-Sky Camera Network - Richard D. Lyons.

96. The Filling over Land of Hurricane Camille, August 17-18, 1969 - Dorothy L. Bradbury.

97.** Tornado Occurrences Related to Overshooting Cloud-Top Heights as Determined from High-Resolution ATS Pictures Showing Anvil Clouds near Salina, Kansas - T. Theodore Fujita.

98.** F P P Tornado Scale and its Applications - T. Theodore Fujita and A. D. Pearson.

99. Preliminary Results of Tornado Watch Experiment 1971 - T. T. Fujita, J. J. Tecson and L. A. Schaal.

100. F-Scale Classification of 1971 Tornadoes - T. Theodore Fujita.

101. Typhoon-Associated Tornadoes in Japan and New Evidence of Suction Vortices in a Tornado near Tokyo - T. Fujita. T. Theodore Fujita.

102. Proposed Mechanism of Suction Spots Accompanied by Tornadoes - T. Theodore Fujita.

103.** A Climatological Study of Cloud Formation over the Atlantic During Winter Monsoon - H. Shitara

104.** Statistical Analysis of 1971 Tornadoes - Edward W. Pearl

105. Estimate of Maximum Windspeeds of Tornadoes in Southernmost Rockies - T. Theodore Fujita.